LA-UR-92-3491

Title: OPTICAL CONSTANTS AND SCATTERING FACTORS FROM REFLECTIVITY MEASUREMENTS: 50 eV TO 5 keV

LA-UR--92-3491

DE93 003750

Author(s). Richard L. Blake, Jeffery C. Davis
Los Alamos National Laboratory

Dale E. Graessle, Thomas H. Burbine
Smithsonian Astrophysical Observatory

Eric M. Gullikson
Lawrence Berkeley Laboratory

MASTER

Submitted to.

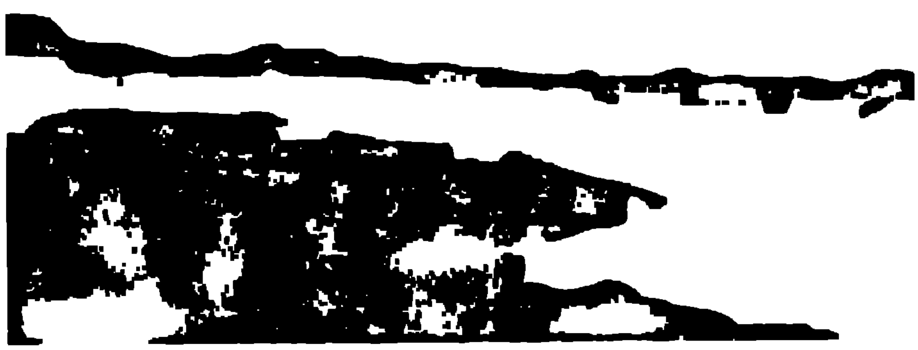

Los Alamos
NATIONAL LABORATORY

Los Alamos National Laboratory, an affirmative action/equal opportunity employer, is operated by the University of California for the U.S. Department of Energy under contract W-7405-ENG-36. By acceptance of this article, the publisher recognizes that the U.S. Government retains a nonexclusive, royalty-free license to publish or reproduce the published form of this contribution, or to allow others to do so, for U.S. Government purposes. The Los Alamos National Laboratory requests that the publisher identify this article as work performed under the auspices of the U.S. Department of Energy.

Optical constants and scattering factors from reflectivity measurements: 50 eV to 5 keV

R. L. Blake[a], J. C. Davis[a], D. E. Graessle[b], T. H Burbine[b], and E. M Gullikson[c]

[a]Los Alamos National Laboratory, MS D410, Los Alamos, NM 87545, USA

[b]Smithsonian Astrophysical Observatory, 60 Garden Street, Cambridge, MA 02138, USA

[c]Lawrence Berkeley Laboratory, Berkeley, CA 94720, USA

Abstract

An improved reflection technique has been introduced to permit more accurate measurements of material optical constants δ and β, the density ρ, and from these the atomic scattering factors f' and f''. Regions of normal and anomolous dispersion can be measured with resolving power 1000 or larger using a portable reflectometer that is moved to any of three beamlines at NSLS or two at CHESS. Herein the reflectometer and measurement techniques are described together with sample characteristics and preliminary results for the Ni L.III edge and the M edges of Au, Pt, and Ir The primary accuracy limiting factors are density determination, accumulation of surface oxides or carbonaceous deposits, and synchrotron orbit stability Each sample must be prepared for the specific energy range to be measured so that model fitting routines have the minimum possible number of free variables

1. INTRODUCTION

This conference brings forth several applications of the need for reliable measurements of material optical constants δ and β, from which atomic scattering factors f' and f'' may be derived There are additional applications in astrophysics, high temperature plasma diagnostics, and synchrotron x-ray optics to name but a few In these fields there is a special need for improved accuracy measurements of f' and f'' for nearly every element over the range 10 eV to 5000 eV

Reflection of xrays from surfaces is described by the well known Fresnel equations in terms of the complex index of refraction $n = 1 - \delta - i\beta$ Material optical constants δ and β are needed in some applications, while in others it is the atomic constants f' and f'' in the atomic scattering factor $f = f_0 + f' + if''$ that are required Most often the absorption part β or f''

is expressed in terms of the mass absorption coefficient μ/ρ. These terms are related for energy E (in eV) by

$$\mu/\rho = 1.0135 \times 10^5 E\beta/\rho = 4.20784 \times 10^7 f''/AE$$

$$f' = 2.4086 \times 10^{-3} E^2 (A/\rho) \delta - Z$$

where ρ is density, A is atomic weight, and Z is atomic number, all pertaining to the reflecting layer. Note that although δ and β may be obtained as material constants by fitting a model to the reflectivity curve, one must independently determine the density ρ in order to specify μ/ρ or f'. Also note that f' obtained from δ will be an experimentally derived number that includes all relativistic and quadrupole terms in theoretical expressions

A new program to derive these "constants" from mirror reflectivity measurements at synchrotrons is herein reported The reflectometer, samples, and measuring technique are outlined along with some preliminary results on the Ni L III and Ir, Pt, and Au M edge regions

2. MEASUREMENT PROGRAM

Reflectance measurements over the wide range of energies desired for optical constants require some special design features Adjustable slits, with low scatter and reflection properties while being opaque to hard xrays, are required before the mirror and at the detector, as shown in Figure 1 Detector and mirror sample must be rotatable independently or

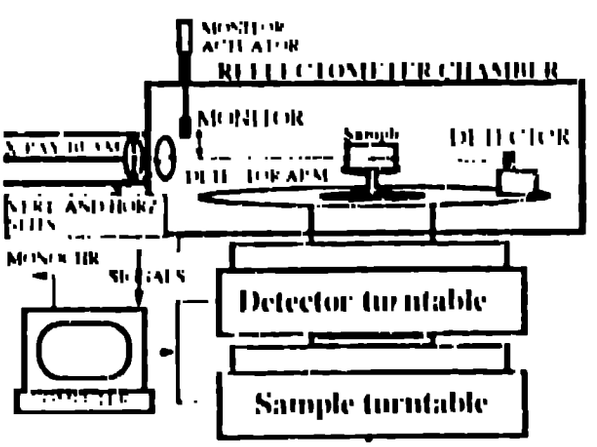

Figure 1 Schematic of reflectometer

together around a common axis Angular accuracy at higher energies must be about one arc sec, for the sample relative to the synchrotron beam, which in turn must not change direction by more than one arc sec due to orbit shifts Re alignment after orbit shifts must be rapid while under vacuum A beam flux monitor must be located between the sample and the reflectometer entrance slit The sample must be capable of being moved out of the beam and

returned accurately to the axis of rotation Samples must be interchangeable on the holder to one arc sec reproducibility With the sample removed and the detector at the direct beam position the detector must be normalized relative to the monitor over all energies to be measured. All operations must be under computer control and executable in a time less than the orbit stability lifetime (usually the refill period) All of these capabilities are provided in vacuum, including internal reflectometer alignment and alignment to the xray beam. The latter is most critical because intermittent orbit shifts cause a change of zero angle of the sample to the beam

The zero angle is determined by the method introduced by Siegbahm and Larrson for x-ray tube spectrographs and used also by Bond for precision lattice constant determinations [1] The dispersion plane is horizontal to meet some of the above criteria Application of the Larrson/Bond method involves measurement of reflectance versus angle symmetrically about the beam direction, first with the sample set to deflect the beam left, then repeated with deflection to the right After one plot is inverted across the beam direction, the amount of shift to make the two overlap is the zero error, which may be corrected immediately in the software or subsequently in the data analysis Shown in Figure 2 are overlays of two such angle scans after inversion but without any shift This example checked orbit stability, which

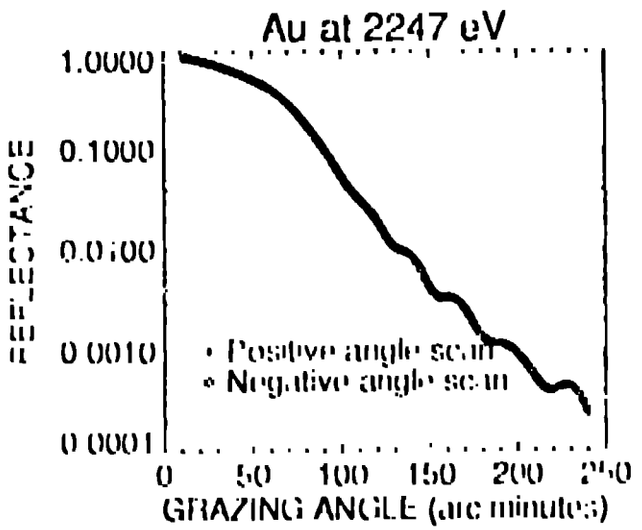

Figure 2 Overlap of left and right detection scans for zero correction (or verification in this case)

changed less than one motor step (0.9 arc sec) since the last alignment The decline of reflectivity above the critical angle and the interference oscillations are compared as the shift is incremented until the rms difference is minimized

Internal reflectometer alignment is executed by a mixture of mechanical and optical techniques [2] Alignment or re alignment to the synchrotron beam requires a combination of left right angle scans and translation across the beam A simple geometrical algorithm can be worked out for each beam line Alignment checks for orbit shifts can be done after each data run on angle scans, if necessary Of more consequence are flux changes arising in monochromator energy scans that do not normalize away at the 0.1 percent level in reflectivity Work continues on solving this problem

Commercially available Si PIN diodes are used without bias for both beam monitor and reflectance detector. Normalization is accomplished by the following steps. With the sample removed from the beam path the detector and monitor are aligned to the direct beam. For each energy position of the monochromator, measurements are taken alternately with monitor and detector for cross calibration, referred to as a normalization scan. Next the mirror sample is placed in the beam path and a reflectance scan is performed versus sample grazing angle θ while the detector is tracked at 2θ. At each angle position measurements are taken alternately with the detector and monitor. Then the reflectivity versus angle is

$$R(\theta) = [D(\theta)/M] / [m(E)/d(E)]$$

where D and M are detector and monitor diode signals from the reflectance scan, and d and m are the same for the normalization scan at the energy of the angular scan. For reflectivity versus energy at fixed angle R(E) is obtained from measurements D(E) and M(E) using the same energy scan range for normalization and reflectance scans. Because the beam flux can change significantly in the 10 seconds between monitor and detector measurements, data quality will be improved by development of a Si mesh detector that can be left in the beam at all times. This detector would also reduce scan times a factor two or more. Sample condition and changes with time are of paramount importance to this method (and to other methods as well). For the work reported here each mirror had a zerodur substrate 6x1.5x1 inches with one 6x1.5 inches surface polished and coated. Substrates were polished to 1/10 wave flatness and less than 5 Å rms microroughness, measured by optical interferometry. All samples included a 50 Å binding layer of Cr between the zerodur and coating. Coatings were made by evaporation or sputtering to 300 Å thickness. Mirrors were stored in plastic containers in dry nitrogen when not in use. Dust was blown off with a pure nitrogen sprayer just before evacuation of the reflectometer. Exposure to room air was allowed during mounting procedures.

After a sample has been mounted and aligned the experiment proceeds with a combination of energy and angle scans. As pointed out by Lengeler [4], absorption edges shift with chemical effects and monochromators often have less than optimum energy calibration. Energy scans locate and clarify features in the mirror reflectance spectrum. Angle scans can then be made at identifiable points in the reflectance spectrum. One derives from the angle scans not only the optical constants but also critical information about density, coating roughness, thickness, and surface contamination [4]. The primary interest is in optical constants from 50 eV to 5000eV, therefore, angle measurements around 7 to 15 keV are used primarily to evaluate sample density in a region of normal dispersion where the optical constants are already well known. This step was not completed on the samples reported herein. Present results are preliminary and may later be refined.

3. PRELIMINARY RESULTS ON Ni L III EDGE

Figure 4 shows an energy scan at fixed angle (14.9 mrad) for a Ni sample that has acquired some surface oxidation as seen by the O K edge at 545 eV. Data were taken on beam line U3C at NSLS with filters to reduce harmonics and stray light. Ni L III, L II, and L I edges are

clearly evident The scatter of data points is much worse on the UV ring than on the x-ray ring for some reasons that will be addressed in the future Detailed energy scans of the LIII

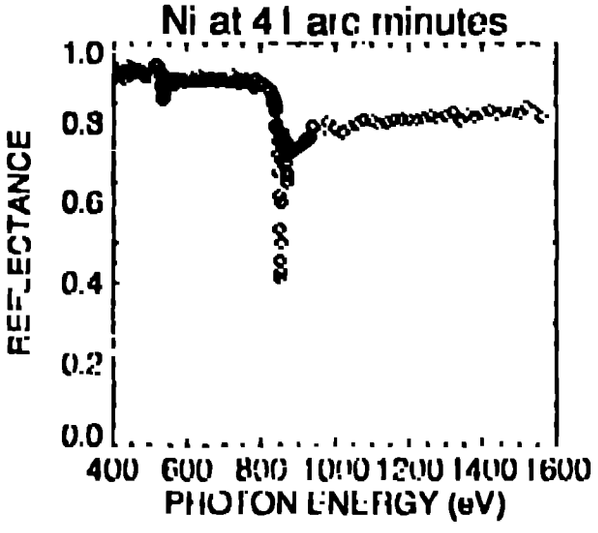

Figure 3. Reflectivity of Ni sample with some oxidation Grazing angle was 41.2 arc minutes Ni LIII, LII, LI edges were identified in repeated scans.

region were made at monochromator slit settings for resolving powers of 300 to 1000 No change could be discerned in the width or shape of the LIII reflectivity dip for resolving power > 500 The LIII edge energy agrees with the electron binding energy 852 7 eV A single scan is given in Figure 4 on which the energies of the angle scans can be identified by

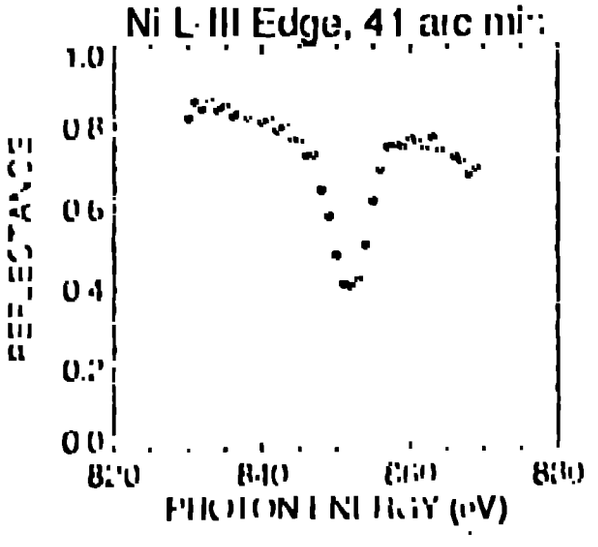

Figure 4 The LIII edge region of Ni in a reflectivity scan at 41 2 arc minutes with resolving power ~ 1000 The lowest point is at 852 eV on the scale of this monochromator Energy steps are 1 eV

counting the 1 eV steps from the lowest point at 852 eV Figure 5 shows these angle scans, which illustrate the changes in reflectivity curves with δ and β At 800 eV where β is low before the edge one gets a critical angle cutoff and high angle oscillations from the interference of rays reflected from the surface with those reflected from the substrate (in this case the Cr layer is the effective substrate) As the energy increases through the edge, β increases causing both a decrease of the reflectivity below the critical angle and damping of the oscillations R becomes almost concave up at the LIII edge (852 eV on this

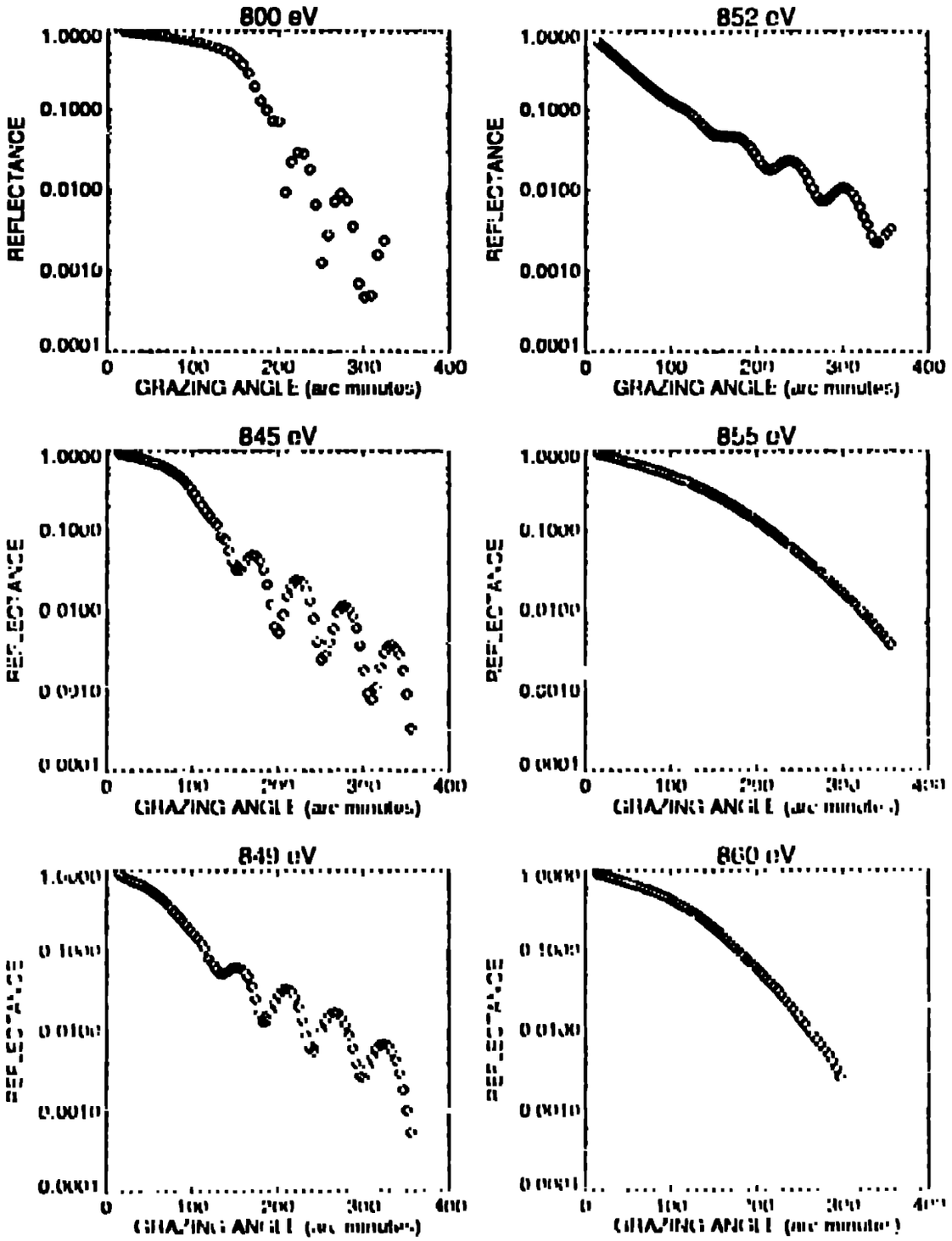

Figure 5 Angle scans at fixed energies across the Ni L III edge region For reference 85.2 eV is the lowest point on Figure 4 It is the L III edge

monochromator). As β continues to increase above the edge the oscillations are completely damped, because the rays penetrate less than the Ni layer thickness, while the curves regain a concave down shape as δ increase with energy above an edge

To achieve good sensitivity on δ and β, use of the maximum possible angle range for Fresnel equation fitting is preferable. Roughness then becomes a key parameter because it also causes damping of oscillations and reduces R(0) at large angles A computer fitting program loaned by David Windt [5] includes roughness and allows for an overlayer and substrate Unfortunately, this program has not yet been modified to use the improved roughness model of Stanglmeier et al [6] Moreover, the Ni and Au samples were used so extensively in vacuum with synchrotron beam illumination that thin surface layers of carbon built up on them, requiring a four layer model. With so many parameters (up to 17) that may be varied the program can converge on a local minimum in chi-squared or sometimes fail to converge Therefore, the analysis was restricted to the range R(0) > 0.1 where the roughness could be set to zero. For these reasons the present results are only approximate. They are included to illustrate the general applicability of reflectivity analysis in the energy region 50 eV to 5 keV

Table 1 contains the best fit values of f and μ/ρ for the six energies of Figure 5, along with the χ^2/degrees of freedom for the best fits, values of f_1 and f_2 for direct comparison to the Henke tables [7], and μ/ρ for four points where we overlap with reference [8]

Table 1
Scattering factors in the Ni LIII region 800 to 860 eV

Energy (eV)		f_1 (el)	f' (el)	f_2 (el)	μ/ρ (cm²/gm)	μ/ρ [8] (cm²/gm)	χ^2/DOF
800[a]	below LIII edge	7.8	-20.5	2.47	2213		8.2 14
845	start LIII edge	4.6	-23.4	2.41	2011		1.9 14
849	increasing f''	2.6	-25.4	2.82	2384	2668	6.2 10
852	near edge energy	-4.7	-32.7	7.40	6223	6506	11.0 8
855	near max f''	3.1	-29.6	17.07	14300	13650	97.1 29
860	between LIII and LII	10.6	-17.4	8.61	7171	9029	10.3 22

[a] μ/ρ should agree with tabulated value [7] 2037

The accuracy of f' is estimated to be ± 3 electrons and μ/ρ is estimated to be ± 20 percent At 800 eV the tabulated value [7] of μ/ρ is the best available - it is nine percent below the value in Table 1 This level of agreement is satisfactory because the sample was analyzed with inclusion of an oxide layer but not with a probable carbon layer, nor with any account of migration of some oxide into the main Ni layer A Ni density of 8.902 was used The

remaining μ/ρ values in Table 1 may be compared to the only measured values known to us [8] After a shift of our energy scale by 0.7 eV to match ref [8], the agreement is within combined uncertainty estimates for μ/ρ

4. PRELIMINARY RESULTS ON Ir, Pt, AND Au M EDGES

Data were taken on beam line X8A at NSLS with Si (111) in a two crystal monochromator. All five M edges have been included in energy scans of Ir, Pt, and Au over the range 2000 to 3500 eV as shown in Figure 6. Both sputtered and electron beam evaporated samples of Au showed the same M edge features Ir and Pt showed the same features except for displacement in energy. Scan steps of 1eV were used near edges; i e the minima in Figure 6.

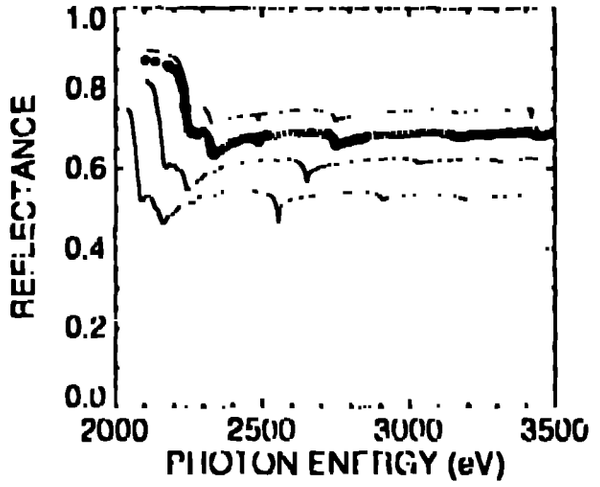

Figure 6. Reflectivity versus energy In order from top down sputtered Au at 7 85 mrad, e-beam evaporated Au at 9.22 mrad, e-beam Pt at 12 0 mrad, and e-beam Ir at 14.9 mrad

Obvious bad points (see 2488 and 3417 eV on the two Au scans) are associated with monochromator glitches that are not removed by normalization These may be ignored The overall quality of these data is much better than the Ni data from the UV ring XAFS features 0 2 percent are reproducible in reflectivity curves of all three materials There is evidence of white line absorption on the MIII edge of Ir and Pt, consistent with the photographic observations of Rogers [9]

In order to get a feel for the optical constants over the entire M edge r gion scans were made at six angles $0 \sim 0_c$, where 0_c is the critical grazing angle of incidence These were treated as 6-point angle scans at every point in the energy scans Results for f' and μ/ρ are given in Figure 7 for Au One cannot expect high accuracy from fits to curves with only six points and four degrees of freedom χ^2/DOF ranges from 0 5/4 to 5/4, except where obvious false trends occur One noisy normalization scan was responsible for this Inflection points on the μ/ρ plot have been used to identify the M edge energies For small grazing angles ~, 15 mrad the inflection points in μ/ρ coincide with the minima in reflectivity, which are better defined for the MIII and MII edges than f' or μ/ρ

Results for the M edge energies are presented in Table 2, where a discrepancy ≈ 40 eV exists between the electron spectroscopy binding energies [10] and the x ray spectroscopic edge energies [9, 11, 12] for the MIV and MV edges Several system checks confirm the

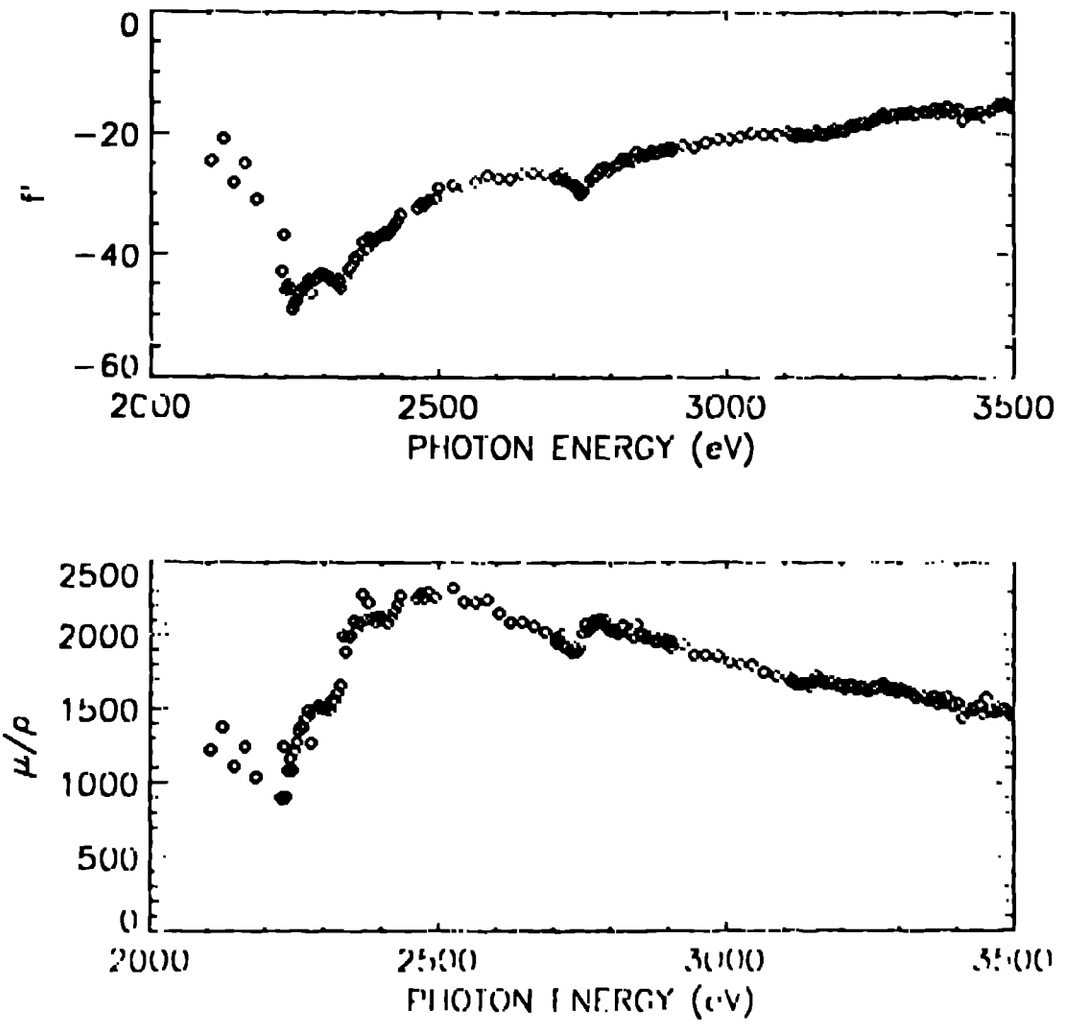

Figure 7 Scattering factors for Au from 6-point angle scans at each energy Note that minima in f' coincide with "inflection points" in μ/ρ

values herein and suggest the difference must be resolved through atomic physics of Au, Pt, and Ir regarding these two edges

These edge energy discrepancies contribute to some divergence between our data in Figure 7 and the Henke tables [7] Therefore, we selected 16 energy points between 2150 eV and 6400 eV for long angle scans to provide an improved set of scattering factors These were analyzed in the same manner as the Ni LIII angle scans, namely, the region $R(0) > 0.2$ was used, all interface roughnesses were set to zero, a carbon overlayer was allowed with adjustable thickness, parameters for the Cr binding layer and substrate were held fixed, and the Au layer was allowed to vary in thickness as well as δ and β Solutions were dependent on initial conditions, which in some cases had to be adjusted to achieve convergent solutions Several alternative approaches to the variables and initial conditions were tried From the range of fits obtained we estimate the accuracy of these preliminary results to be ± 5 percent

on δ and ± 10 percent on β. In the conversion from δ and β to f' and μ/ρ a density of 19.32 gm/cm^3 was used, since we have not yet been able to use the higher energy beam line to evaluate the Au density independently. Results on f' and μ/ρ for one Au sample are given in Table 3 for the 16 energies where angle scans were performed. The uncertainty in f' is estimated to be ± 2 electrons.

Table 2
M edge energies in eV for Ir, Pt, and Au

Edge	Electron spectroscopy binding energy [10] / X-ray spectroscopy edge energy		
	Ir	Pt	Au
MV	2040 / 2092 ± 5	2122 / 2174 ± 5	2206 / 2247 ± 5
	--	2171 [11]	2252 [11]
	2080 [9]	2162 [9]	2245 [12]
MIV	2116 / 2161 ± 5	2202 / 2248 ± 5	2291 / 2330 ± 5
	--	2252 [11]	2333 [11]
	2155 [9]	2238 [9]	--
MIII	2551 / 2555 ± 5	2645 / 2652 ± 5	2743 / 2748 ± 5
	--	2651 [11]	2755 [11]
	2556 [9]	2653 [9]	--
MII	2909 / 2917 ± 5	3026 / 3037 ± 5	3148 / 3148 ± 5
	2904 [9]	3035 [11]	--
MI	3174 / 3193 ± 10	3296 / 3315 ± 10	3425 / 3425 ± 10
	--	3313 [11]	3441 [11]
	--	3317 [9]	--

5. DISCUSSION

X-ray spectroscopic edge energies agree with electron spectroscopy binding energies for three Ni L edges and three of five M edges for Ir, Pt, and Au. The difference of 40 to 50 eV for the MV and MIV edges of Ir, Pt, and Au must be explained through atomic physics rather than experimental error. There is no evidence of white line absorption on the MV and MIV edges.

Table 3
Scattering factors in the Au M region and higher

ENERGY (eV)		δ / δ_H[a] (1E - 4)	β / β_H[a] (1E - 5)	f[b] (electrons)	μ / ρ[b] (cm2/gm)	χ^2 / DOF
2150	*Below MV edge	3.64 / 2.5	7.54 / 8.99	-37.7	850	1.45 / 30
2220	Begin increasing MV β	2.75 / 0.84	7.27 / 12.63	-45.7	847	2.6 / 24
2247	MV edge	2.52 / 2.33	14.4 / 19.2	-47.8	1697	1.2 / 21
2294	XAFS between MV and MIV	2.73 / 2.80	16.36 / 25.8	-43.7	1969	8.5 / 22
2316	Before β rise to MIV edge	2.46 / 2.88	15.66 / 28.4	-46.6	1903	4.0 / 20
2330	MIV edge	2.47 / 2.98	17.3 / 27.8	-46.1	2115	3.4 / 19
2350	Above MIV edge, β rising	2.72 / 3.12	17.4 / 27.0	-42.1	2145	3.25 / 21
2370	Max MIV β	2.78 / 3.26	18.4 / 26.2	-40.7	2288	3.6 / 21
2400	In MIV XAFS	2.88 / 3.34	17.4 / 25.1	-38.3	2191	18.4 / 22
2480	In MIV XAFS	2.98 / 3.42	16.8 / 22.5	-34.0	2186	12.6 / 22
2600	*Smooth reg btwn MIV&MIII	2.86 / 3.32	14.8 / 19.2	-31.5	2019	4.0 / 23
2720	Before rise of MIII β	2.64 / 3.04	12.7 / 16.6	-31.0	1812	0.35 / 21
3000	*Smooth reg btwn MIII&MII	2.47 / 2.86	11.1 / 13.6	-24.4	1747	0.61 / 20
3125	Before rise of MII β	2.33 / 2.68	10.3 / 12.0	-23.1	1689	0.27 / 20
5050	*Away from edges	1.15 / 1.22	2.59 / 2.61	-8.40	676	0.73 / 8
6400	*Sensitive to Cr binding layer	0.72 / 0.75	1.13 / 1.09	-6.58	379	0.125 / 5

* values should agree with tabulations for β_H in [7]

[a] δ_H not useful 2150 to ~ 3500 eV, β_H not useful near edges

[b] based on ρ = 19.32

It has become routine to compare low energy scattering factors with the Henke tables because they represent a semi-empirical compilation of available data. One expects to obtain good μ/ρ values from the Henke tables just below and well above an absorption edge. The Ni data at 800 eV presented here agree within estimated experimental error, thus giving confidence in the values in the LIII edge region. This confidence is further enhanced by the agreement with ref. [8] at four points within the LIII resonance feature. A significant difference at 2150 and 2220 eV for Au is at least in part explained by the edge energy discrepancy. The present results at 5000 and 6400 eV agree with Henke tables within 3 5 percent. The remaining values within the M region cannot be given the same accuracy estimate, because the values are very sensitive to initial conditions and model parameters in the fitting routine. At least the reflectivity program for optical constants in the 50 eV to 5 keV range has been proven realistic.

6. REFERENCES

1. R L. Blake, J.C. Davis, P.P. Gong, D.E. Graessle and W. Rudermann, SPIE, Vol. 1546 (1991) 392.

2. J L. Thomson, in X-Ray Spectroscopy, ed. by L.Z. Azarov, McGraw-Hill, New York (1974) 26.

3. M Krumrey and E. Tegeler, Rev. Sci Instrum , 63 (1992) 797.

4. this conference and [5].

5. D.L. Windt, Ph D. Thesis, Univ. of Colorado-Boulder (1986) and Applied Optics, 27 (1988) 279.

6. F. Stranglmeier, B. Lengeler, W. Weber, H. Gobel and M Schuster, Acta Cryst , A48 (1992) 626.

7. B L. Henke, P Lee, T.J. Tanaka, R L. Shimabukuro and B K Fujikawa, Atomic Data and Nuclear Data Tables, 27 (1982) and updated version to be published

8. N K Del Grande, SPIE Proc , Vol 911 (1988) 6.

9 R A Rogers, Phys Rev , 30 (1927) 747 and 29 (1927) 205

10. J A Bearden and A F. Burr, Rev Mod Phys , 39 (1967) 125 and A Fahlman and S Hagstrom, Ark Fysik , 27 (1964) 69

11 A J M Johnson, Phys Rev , 33 (1929) 120

12 J M Andre, R Barchewitz, A Maquet and R Marmoret, Phys Rev B, 30 (1984) 6576